PNAS
www.pnas.org

Supplementary Information for

LRRK2 plays essential roles in maintaining lung homeostasis and preventing the development of pulmonary fibrosis

Yujie Tian[1], Jiaoyan Lv[1], Ziyan Su, Tao Wu, Xiaoguang Li, Xiaoyu Hu, Jianhong Zhang, Li Wu[2]

[1]These authors contributed equally to this work: Yujie Tian and Jiaoyan Lv.

[2]To whom correspondence should be addressed. Email: wuli@tsinghua.edu.cn.

This PDF file includes:

SI Materials and Methods

Micro-computed tomography (micro-CT) analysis. Mice were anesthetized with isoflurane and then scanned and analyzed with high-resolution micro-CT (Quantum GX micro-CT, Perkin Elmer). The scanner was set at 90 kV, 88 μA, 36 mm FOV, and a resolution of 72 μm/pixel.

Pulmonary function test. Mice were anesthetized with 1% pentobarbital. After being tracheotomized and cannulated, mice were connected to the ventilator of the DSI's Buxco® FinePointe Series Resistance and Compliance (RC) sites. After a period of resting, the lung resistance (RL), dynamic lung compliance (Cdyn), and minute ventilation volume (MV) were recorded.

BM chimeric mice. For generating reciprocal BM chimeric mice, approximately 6- to 8-week-old WT or *Lrrk2*$^{-/-}$ recipient mice were lethally irradiated with two doses of 5 Gy, each approximately 2 hours apart. Donor WT mice or *Lrrk2*$^{-/-}$ mice were sacrificed and BM cells were harvested from both femurs and tibias under sterile conditions. After removing erythrocytes by RCRB, approximately 2 × 10^6 unfractionated BM cells in 250 μl of PBS were injected intravenously into each recipient mice via tail vein. Four groups of *Lrrk2*$^{-/-}$ chimera mice were generated: WT → WT, *Lrrk2*$^{-/-}$ → WT, WT → *Lrrk2*$^{-/-}$, and *Lrrk2*$^{-/-}$ → *Lrrk2*$^{-/-}$. For blocking CCL2/CCR2 signaling, WT and *Ccr2*$^{-/-}$ mice were used as donors and four groups of BM chimeric mice were similarly generated as follows: WT → WT, *Ccr2*$^{-/-}$ → WT, *Lrrk2*$^{-/-}$ → *Lrrk2*$^{-/-}$, and *Ccr2*$^{-/-}$ → *Lrrk2*$^{-/-}$. BM chimeric mice were subjected to BIPF at 6 weeks post BM cell transfer.

Lung histopathological analysis. Lung tissues were removed from the chest and fixed in paraformaldehyde overnight, and then embedded in paraffin for sectioning. H&E staining and Masson's trichrome staining were performed for histopathological analysis and measurement of lung collagen deposition. The severity of pulmonary fibrosis was assessed according to the Ashcroft score, as previously described (1). Immunohistochemical staining of α-smooth muscle actin (α-SMA, ab32575, Abcam), collagen I (Col-I, GB11022-1, Servicebio) and surfactant protein C (SP-C, ab211326, Abcam) was performed on paraffin-embedded lung sections. All microscopic analyses were conducted by Axio Scan.Z1 (Zeiss).

ELISA. BALF was collected with 0.5 ml of cold PBS through tracheal intubation and supernatant was obtained by centrifugation for measurement of protein concentration and cytokine production. The concentrations of IL-6 (eBioscience), activated TGF-β1 (R&D Systems), CCL2, CXCL1 (multiSciences), and CXCL2 (R&D Systems) in BALF were quantified by ELISA. Lung tissues were homogenized in 0.5 ml of cold PBS containing proteinase inhibitor cocktail (Bimake) on ice. Lung homogenates were centrifuged, and supernatants were collected for measuring the concentrations of IL-13, IL-17A, IFNγ (eBioscience), CXCL1, and CXCL2 by ELISA. All measurements were conducted according to the manufacturers' instructions.

Sircol assay. The total collagen content of frozen caudal lobes from the right lung of each animal was determined using the Sircol collagen assay (Biocolor Ltd., Belfast, UK) according to the manufacturer's instructions as previously described (2). Briefly, lung tissues were homogenized in 500 μl RIPA Lysis and Extraction Buffer (Thermo) containing protease inhibitor cocktail (Sigma). Homogenates were centrifuged (12,000 g, 10 minutes, 4 °C) to collect the supernatant. Commercial Sircol dye reagent (500 μl) was added to each lung homogenate (50 μl) and incubated for 30 minutes on a rotator at room temperature. After centrifugation at 12,000 g for 10 minutes, the collagen-dye pellets were washed with acid-salt wash reagent, and dissolved in 500 μl of alkali reagent. Absorbance was measured at 540 nm in a ELx800 Microplate Reader (BioTek). Collagen concentrations were calculated using a standard curve generating using the collagen standard by the manufacturer.

RNA extraction and quantitative RT-PCR. RNA of lung tissues or sorted cells was extracted by TRIzol Reagent (Invitrogen), and cDNA was generated by using PrimeScript™ RT Master Mix

(Takara). A PowerUp™ SYBR™ Green Master Mix (Applied Biosystems) was used, and samples were run on an HT7900 (Applied Biosystems) quantitative PCR machine. Primers are listed in the *SI Appendix*, Table S2. Gene expression was normalized to the expression of house-keeping gene *Actb* and expressed in Arbitrary Units.

Protein extraction and Western blot analysis. Lung tissues and sorted cells were lysed in cold RIPA Lysis and Extraction Buffer (Thermo) supplemented with protease inhibitor cocktail (Sigma) and phosphatase inhibitor cocktail (Bimake). After incubation for 30 minutes on ice with rotating, supernatants were collected after centrifugation (12,000 rpm, 15 minutes, 4 °C) and protein concentrations were measured by using BCA Protein Assay (Pierce). Total protein was denatured and loaded into the SDS-PAGE, and then transferred the protein from the gel to the activated PVDF membranes. After blocked with the blocking buffer, the membranes were hybridized overnight with appropriate primary antibodies (LRRK2, NB300-268, Novus; p62, A5180, Bimake; LC3B, A5202, Bimake; p53, 2524, CST; p21, ab188224, Abcam; ATG5, 12944, CST; ATG16L1, 8089, CST; ERK, sc-94, Santa Cruz; p-ERK, A5036, Bimake; JNK, 9258, CST; p-JNK, 4668, CST; mTOR, 2983, CST; p-mTOR, ab109268, Abcam; β-Catenin, ab32572, Abcam; β-actin, 3700, CST). Membranes were incubated in the SuperSignal* West Pico Chemiluminescent Substrate (Pierce), and imaging was carried out with Amersham Imager 600 System (GE). Quantifications of specific protein bands were conducted with the Image J software (https://imagej.nih.gov/ij/).

Transmission electron microscope. Sort-purified AT2 cells were washed by PBS and collected into microcentrifuge tubes. After centrifuging, cells were fixed by 2.5% glutaraldehyde overnight at 4 °C. Fixed cells were dehydrated, embedded, and sliced. Ultrathin sections were examined with a Tecnai T12 transmission electron microscope (FEI).

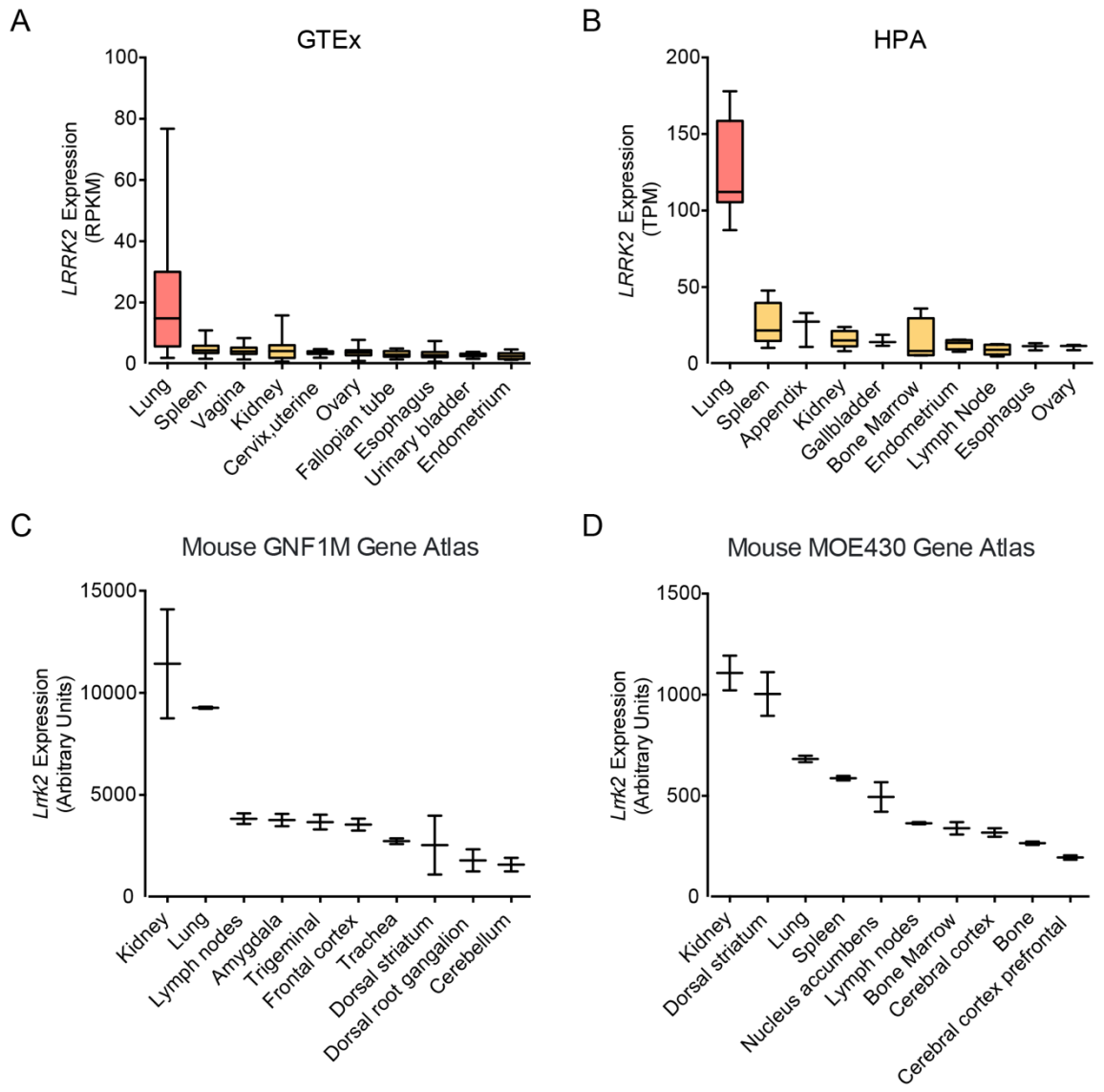

Fig. S1. The expression of LRRK2 in human and mouse tissues. (*A* and *B*) *LRRK2* mRNA levels in healthy human tissues were analyzed by deriving transcriptomic data from (*A*) GTEx dataset (3) and (*B*) HPA dataset (4). *LRRK2* expression in the lung was outlined by a salmon bar. (*C* and *D*) *Lrrk2* mRNA levels in normal *C57BL/6* mouse tissues were analyzed by deriving transcriptomic data from (*C*) Mouse GNF1M Gene Atlas dataset (GSE1133) (5) and (*D*) Mouse MOE430 Gene Atlas dataset (GSE10246) (6) by using BioGPS (http://biogps.org) (7). Top 10 tissues with the highest expression of LRRK2 were shown. Data are plotted by box-and-whisker diagrams, and whiskers represent min to max.

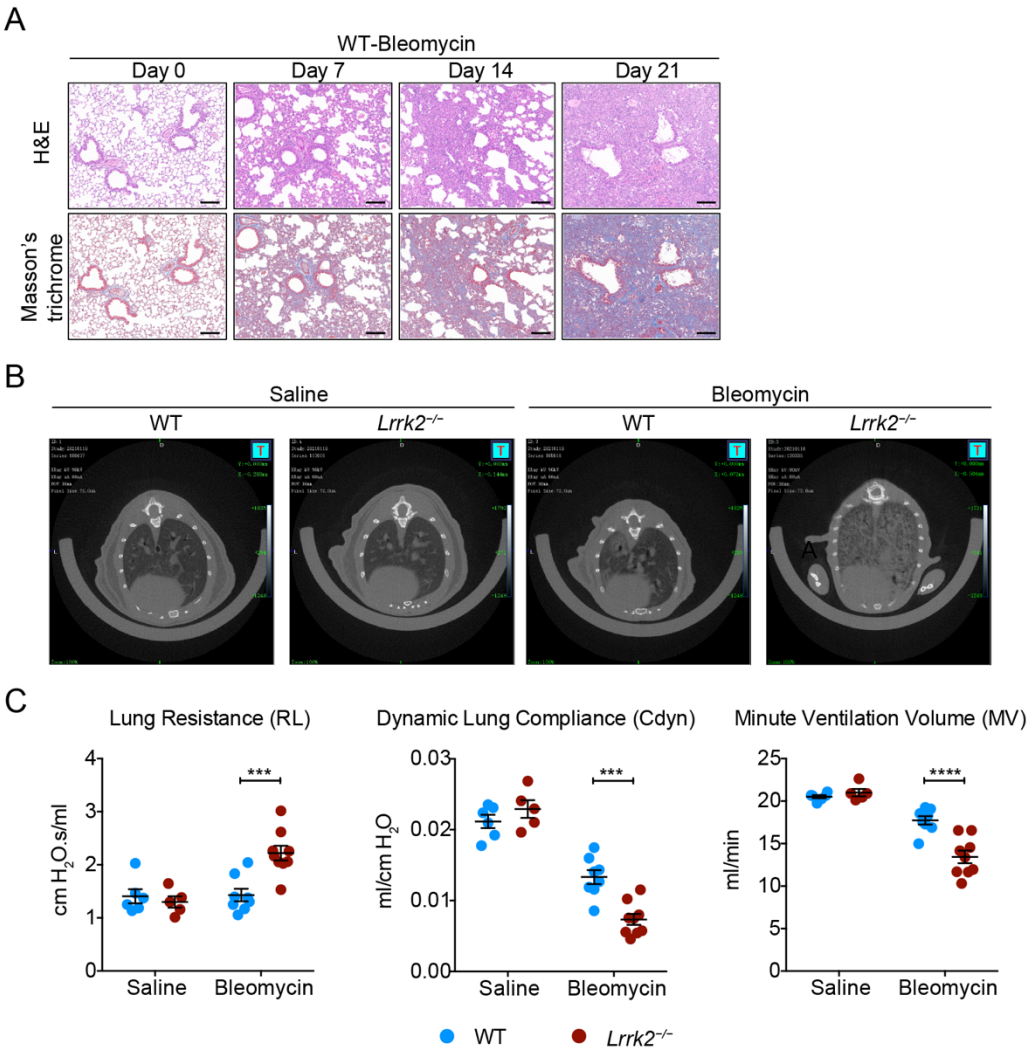

Fig. S2. LRRK2 deficiency in mice exacerbated pulmonary fibrosis and impaired pulmonary function post bleomycin exposure. (*A*) Representative images of the H&E- and Masson's trichrome-stained lung sections of WT mice in indicated time points after bleomycin administration (n = 3-4 for each time point). Scale bars: 100 μm. (*B* and *C*) WT and *Lrrk2*$^{-/-}$ male mice were challenged with saline or bleomycin for 10 days and were subjected to micro-CT analysis and pulmonary function test. (*B*) Representative micro-CT images of lungs were shown (n = 3-4 per group). (*C*) Lung resistance (RL), dynamic lung compliance (Cdyn), and minute ventilation volume (MV) were recorded. Data are shown as mean ± SEM (n = 5-9). Differences were considered significant at $P < 0.05$, ***$P < 0.001$, ****$P < 0.0001$, by two-way ANOVA followed by Bonferroni's multiple comparison test.

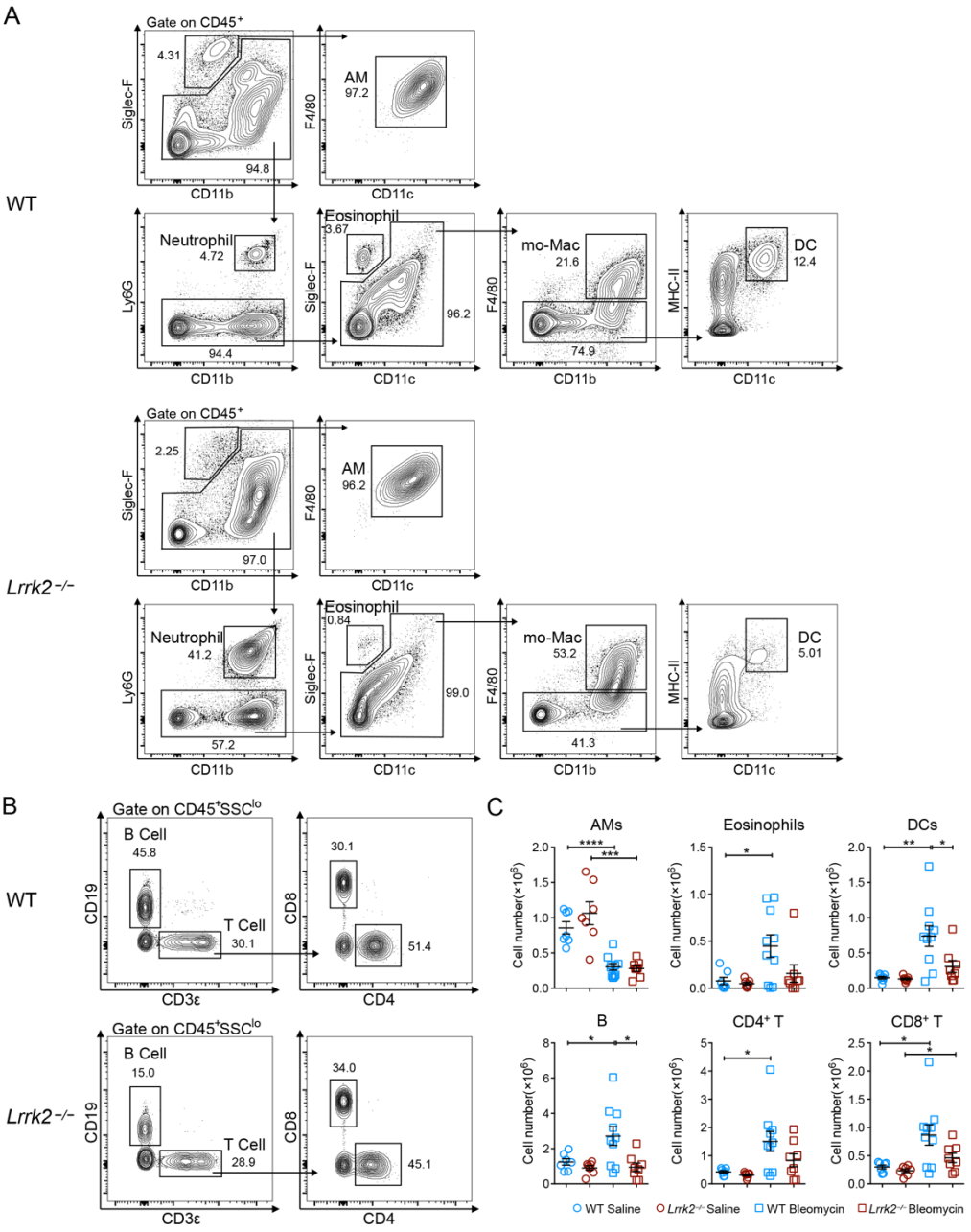

Fig. S3. Flow cytometric analysis of CD45⁺ populations in lung tissues. (*A* and *B*) Gating strategy used to identify (*A*) myeloid cell subsets and (*B*) lymphocytes in enzymatically digested lung tissues from saline- or bleomycin-treated WT and *Lrrk2*$^{-/-}$ mice at day 7. Immune cells were gated on CD45⁺ following the removal of doublets and dead cells. Different myeloid cell subsets were identified based on the expression of CD11c, Siglec-F, CD11b, Ly6G, F4/80, and MHC-II. Lymphocytes were gated on SSC^{lo} cells and then B and T cell subsets were identified based on the expression of CD3ε, CD19, CD4, and CD8. (*C*) Numbers of AMs, eosinophils, DCs and lymphocytes in lung tissues were quantified based on flow cytometry profiling. Data are shown as mean ± SEM (n = 7-10) and are integrated from three independent experiments; *P < 0.05, **P < 0.01, ***P < 0.001, ****P < 0.0001, by two-tailed Student's t-test.

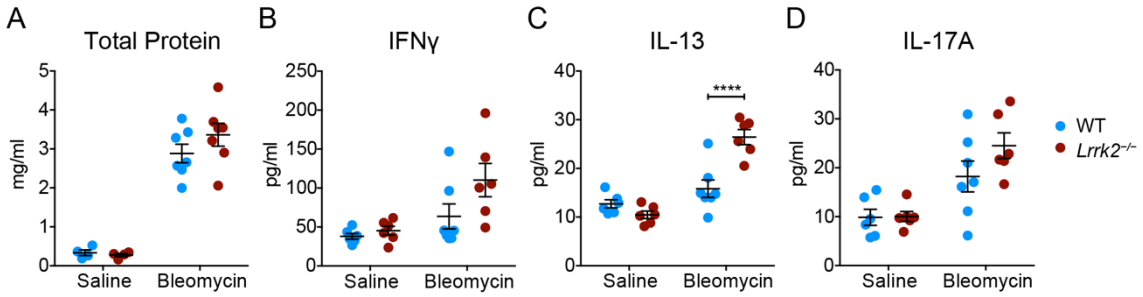

Fig. S4. LRRK2 deficiency promoted IL-13 production during bleomycin-induced lung injury. WT and *Lrrk2*$^{-/-}$ male mice were challenged with saline or 1.5 mg/kg bleomycin, BALF and lungs were harvested at day 7 for the following analyses. (*A*) Total protein concentration in BALF from WT and *Lrrk2*$^{-/-}$ mice were quantified. (*B-D*) ELISA analysis of (*B*) IFNγ, (*C*) IL-13, and (*D*) IL-17A expressions in lung tissues from WT and *Lrrk2*$^{-/-}$ mice were quantified. Data are shown as mean ± SEM (*n* = 4-7 for *A*; *n* = 6-7 for *B-D*) and are integrated from two independent experiments. Differences were considered significant at $P < 0.05$, ****$P < 0.0001$, by two-way ANOVA followed by Bonferroni's multiple comparison test.

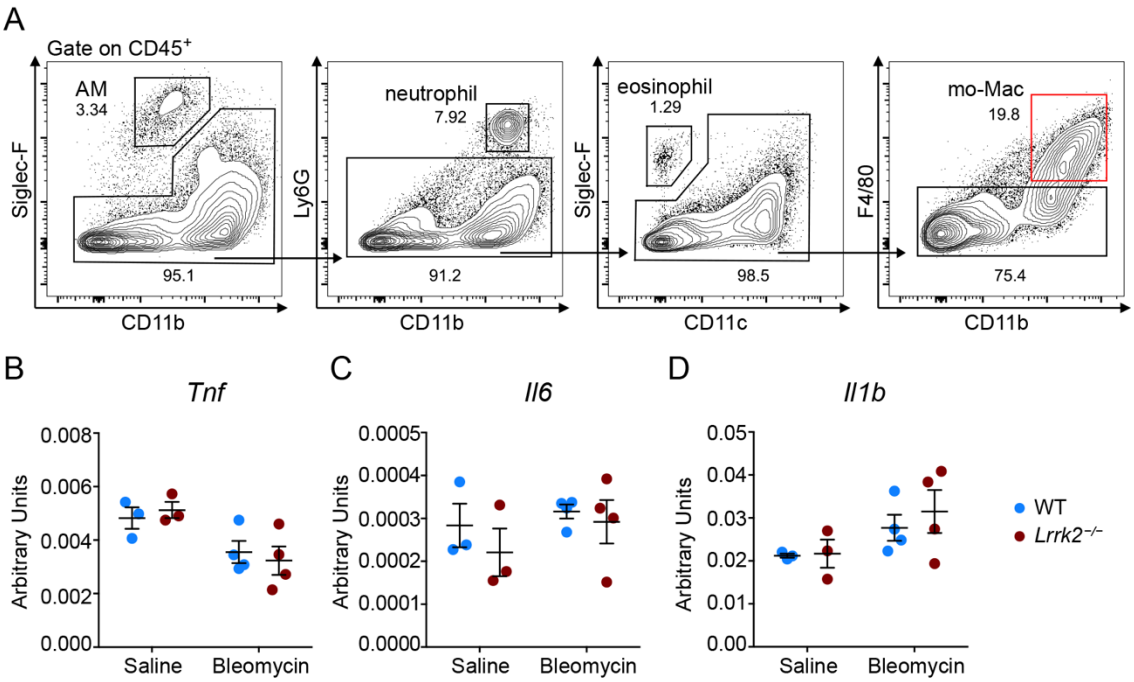

Fig. S5. LRRK2 was dispensable for classical macrophage activation in BIPF. WT and *Lrrk2*$^{-/-}$ male mice were treated with saline or 1.5 mg/kg bleomycin for 7 days, and mo-Macs from lung tissues were isolated for the following analyses. (*A*) Gating strategy used to isolate mo-Macs from mouse lung tissues by flow cytometer. (*B-D*) Quantitative analyses of mRNA levels of proinflammatory factors associated with classical macrophage activation, including (*B*) *Tnf*, (*C*) *Il6*, and (*D*) *Il1b*, by qRT-PCR. Data are shown as mean ± SEM (*n* = 3-4) and are representative of three independent experiments. Differences were considered significant at $P < 0.05$, by two-way ANOVA followed by Bonferroni's multiple comparison test.

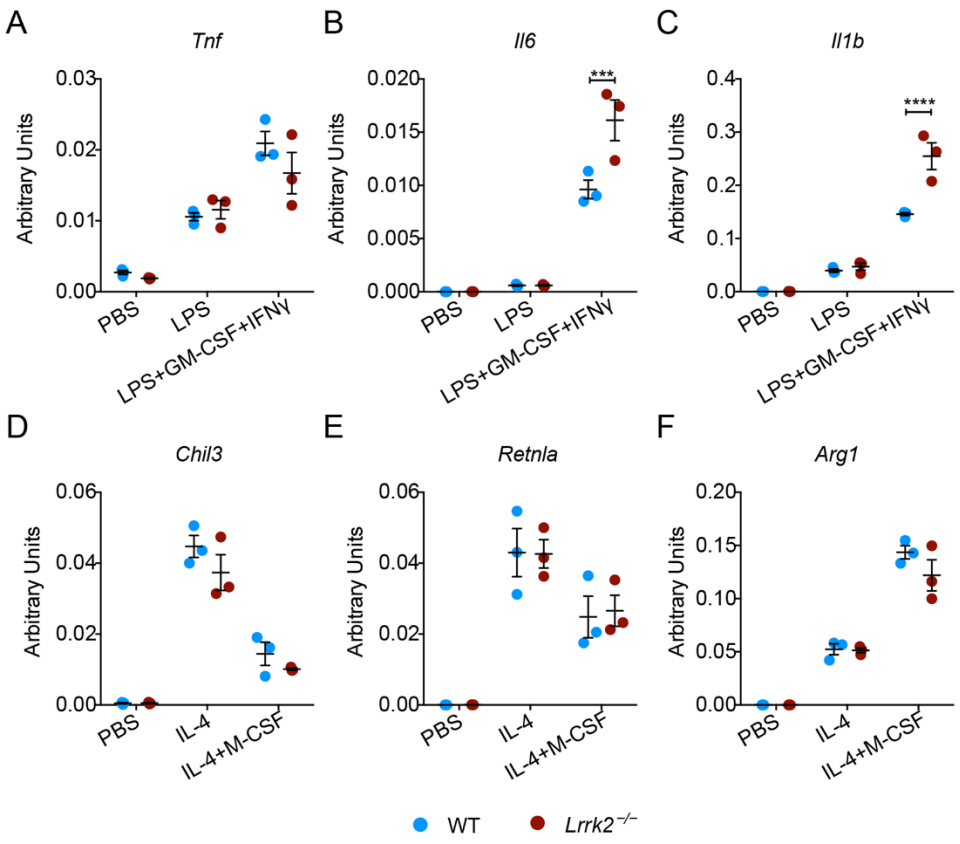

Fig. S6. LRRK2 deficiency promoted classical macrophage polarization *in vitro*. (*A-C*) BMDMs from WT and *Lrrk2*$^{-/-}$ mice were stimulated with 100 ng/ml LPS or in combination of 100 ng/ml LPS,20 ng/ml GM-CSF, and 10 ng/ml IFNγ for 24 h. The relative mRNA levels of classical macrophage activation markers, including (*A*) *Tnf*, (*B*) *Il6*, and (*C*) *Il1b*, were assessed by qRT-PCR. (*D-F*) BMDMs from WT and *Lrrk2*$^{-/-}$ mice were stimulated with 10 ng/ml IL-4 or 10 ng/ml IL-4 and 20 ng/ml M-CSF for 24 h. The relative mRNA levels of alternatively activated macrophage markers, including (*D*) *Chil3*, (*E*) *Retnla*, and (*F*) *Arg1*, were assessed by qRT-PCR. All expression values were normalized to *Actb*. Data shown are means ± SEM (n = 3) and are representative of three independent experiments. ***P < 0.001, ****P < 0.0001, by two-way ANOVA followed by Bonferroni's multiple comparison test.

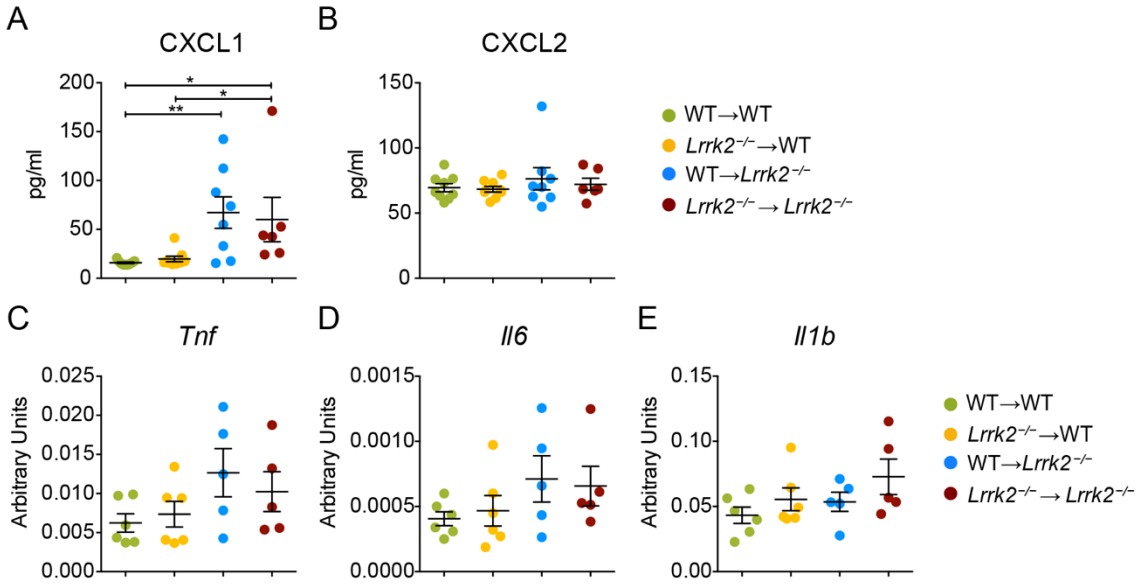

Fig. S7. Expression levels of neutrophil chemoattractants in lung and the mo-Mac-derived proinflammatory cytokines in bleomycin-treated BM chimeric mice. The four groups of BM chimeric mice were challenged with 1.5 mg/kg bleomycin for 7 days, lung tissues were harvested for the following analyses. (*A* and *B*) ELISA analysis of neutrophil chemoattractant (*A*) CXCL1 and (*B*) CXCL2 levels in lung tissues. (*C-E*) Quantification of relative mRNA expression levels of proinflammatory cytokines including (*C*) *Tnf*, (*D*) *Il6*, and (*E*) *Il1b* by qRT-PCR in isolated lung mo-Macs. Data are shown as mean ± SEM (n = 6-9 for *A* and *B*; n = 5-6 for *C-E*) and are integrated from (*A* and *B*) or representative of (*C-E*) at least two independent experiments. **P* < 0.05, ***P* < 0.01, by two-tailed Student's *t*-test.

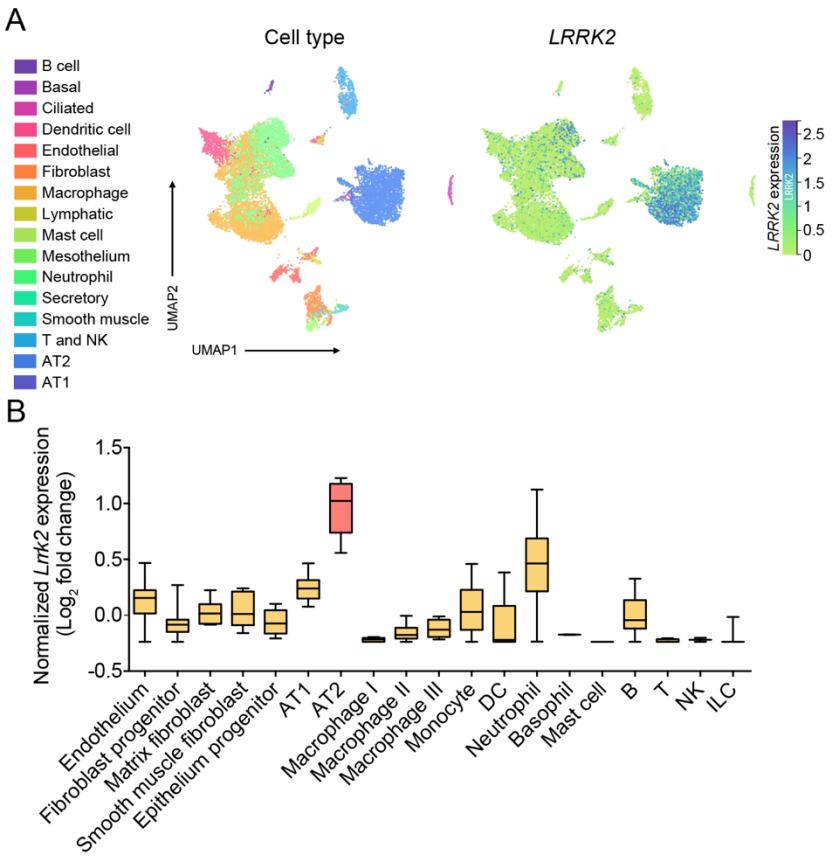

Fig. S8. LRRK2 is predominantly expressed by AT2 cells in human and mouse lungs. (*A*) UMAP plot displaying the major resident cell types in the human respiratory tree (left) and showing expression of *LRRK2* in each cell cluster (right) generated by covid19cellatlas.org (8). (*B*) *Lrrk2* expression in different mouse lung cell types was plotted by analyzing a published whole-lung scRNA-Seq dataset (GSE119228) (9).

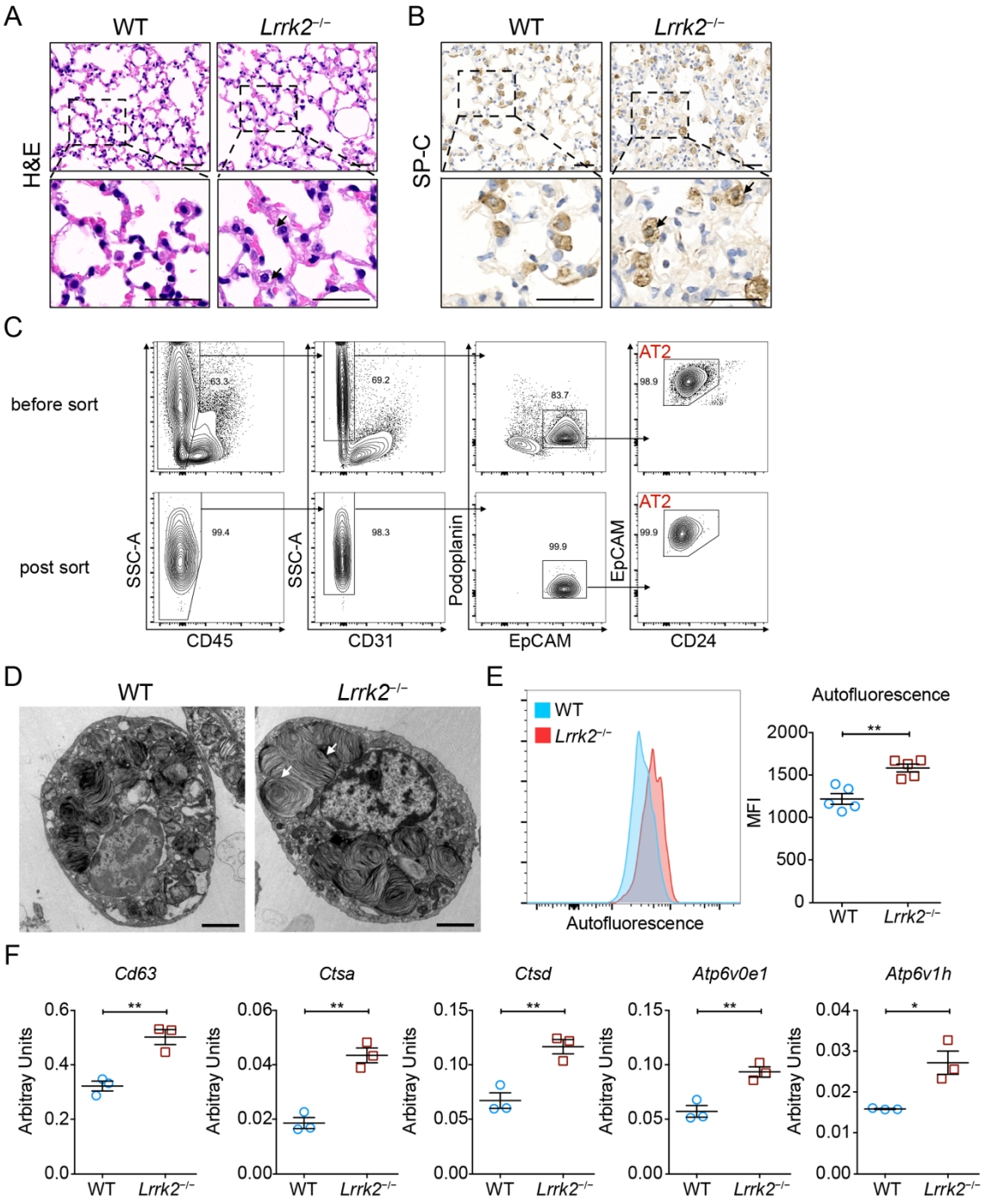

Fig. S9. Loss of LRRK2 altered homeostasis of AT2 cells characterized by enlarged lamellar bodies. (*A*) Representative images of H&E-stained lung sections. Scale bars: 20 μm. (*B*) Representative immunohistochemical analysis of SP-C-expressed AT2 cells in lung sections. Scale bars: 20 μm. The black arrows in (*A*) and (*B*) indicate the vacuoles formed in AT2 cells from LRRK2-deficient mice. (*C*) Gating strategy used to isolate AT2 cells from mouse lung tissues by flow cytometer. (*D*) AT2 cells isolated from WT and LRRK2-deficient mice were evaluated by transmission electronic microscopy (original magnification: 6000×). Scale bars: 2 μm. The white arrows indicate the

enlarged lamellar bodies in AT2 cells from LRRK2-deficient mice. (*E*) Autofluorescence of WT and LRRK2-deficient AT2 cells was measured by flow cytometry. Representative flow cytometry histogram and mean fluorescence intensity (MFI) were shown. (*F*) The relative mRNA expression levels of representative lamellar body-associated genes in WT and LRRK2-deficient AT2 cells were determined by qRT-PCR, and all expression values were normalized to *Actb*. Data are shown as mean ± SEM ($n = 5$ for *E*; $n = 3$ for *F*). $^{*}P < 0.05$, $^{**}P < 0.01$, by two-tailed Student's *t*-test.

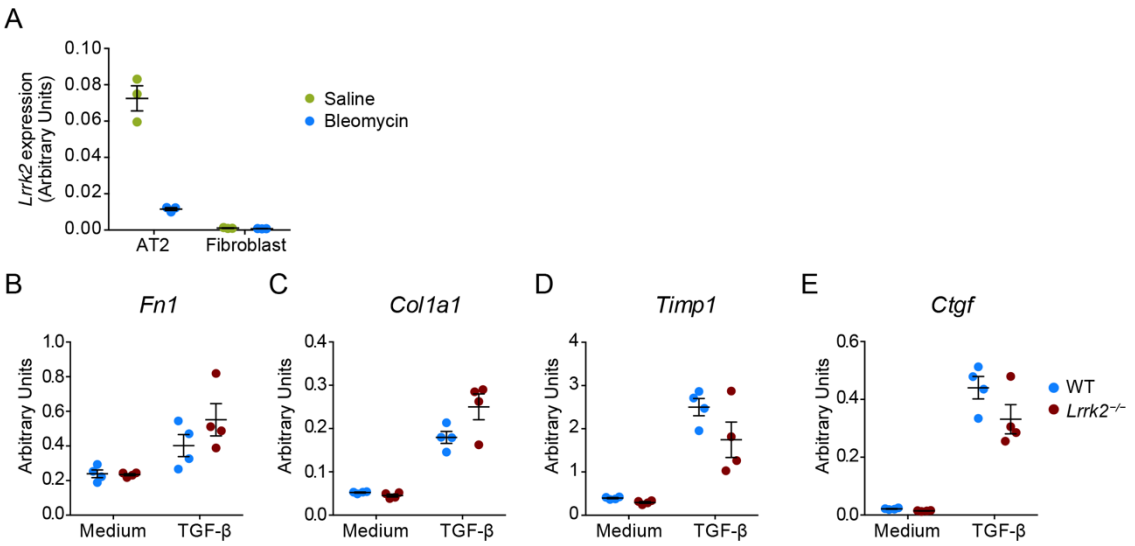

Fig. S10. LRRK2 was minimally expressed in lung fibroblasts and dispensable for their activation in vitro. (*A*) *Lrrk2* expression in AT2 cells and lung fibroblasts isolated from saline- or bleomycin-treated WT mice at day 7 measured by qRT-PCR. (*B-E*) Primary lung fibroblasts isolated from WT and *Lrrk2*$^{-/-}$ mice were serum-starved overnight and stimulated with 10 ng/ml TGF-β for 48 h. The relative mRNA expression levels of representative fibroblast activation markers, including (*B*) *Fn1*, (*C*) *Col1a1*, (*D*) *Timp1*, and (*E*) *Ctgf*, were determined by qRT-PCR. Data are shown as mean ± SEM ($n = 3$ for *A*; $n = 4$ for *B*) and are representative of three independent experiments. Differences were considered significant at $P < 0.05$, by two-way ANOVA followed by Bonferroni's multiple comparison test (*B-E*).

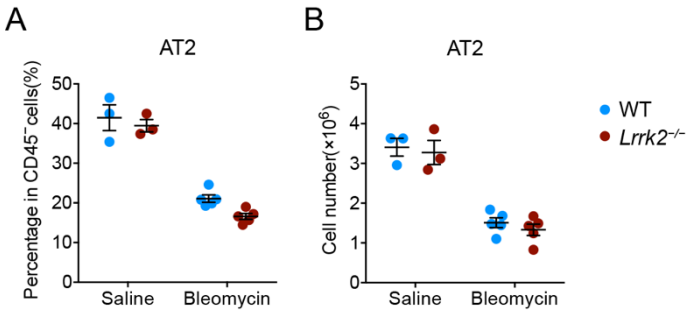

Fig. S11. LRRK2 deficiency has no effect on the magnitude of AT2 cells in lung. WT and *Lrrk2*$^{-/-}$ mice were treated with saline or 1.2 mg/kg bleomycin for 7 days. (*A*) The percentage and (*B*) the number of AT2 cells in lung were examined by flow cytometric analysis. Data are shown as mean ± SEM (n = 3-5). Differences were considered significant at $P < 0.05$, by two-way ANOVA followed by Bonferroni's multiple comparison test.

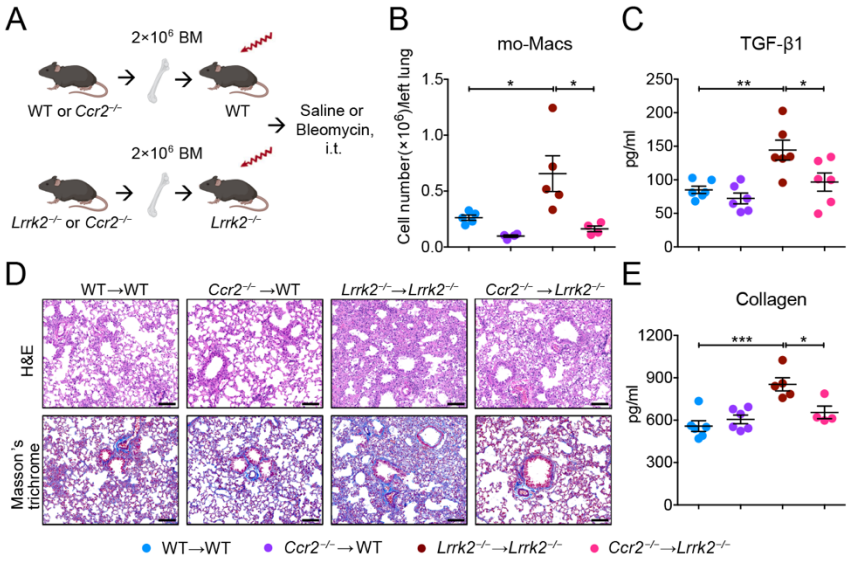

Fig. S12. Blocking the CCL2/CCR2 axis attenuated recruitment of mo-Macs and profibrotic responses in LRRK2-deficient mice. (*A*) Scheme of BM chimeric mice construction for blocking the CCL2/CCR2 axis. Icons were created with BioRender.com. (*B* and *C*) Lung tissues and BALF from bleomycin-treated BM chimeric mice were harvested at day 7 for the following analyses. (*B*) Numbers of infiltrated mo-Macs in lung tissues were quantified by flow cytometry. (*C*) TGF-β1 expression in BALF were quantified by ELISA analysis. The four groups of BM chimeric mice were treated with 1.5 mg/kg bleomycin for 9 days. (*D*) Representative images of H&E and Masson's trichrome staining of lung tissue sections. Scale bars, 100 μm. (*E*) Quantification of collagen content in lung homogenates using the Sircol Assay. Data are shown as mean ± SEM (n = 4-6) and are representative of two to three independent experiments. *P < 0.05, **P < 0.01, ***P < 0.001, by two-tailed Student's t-test.

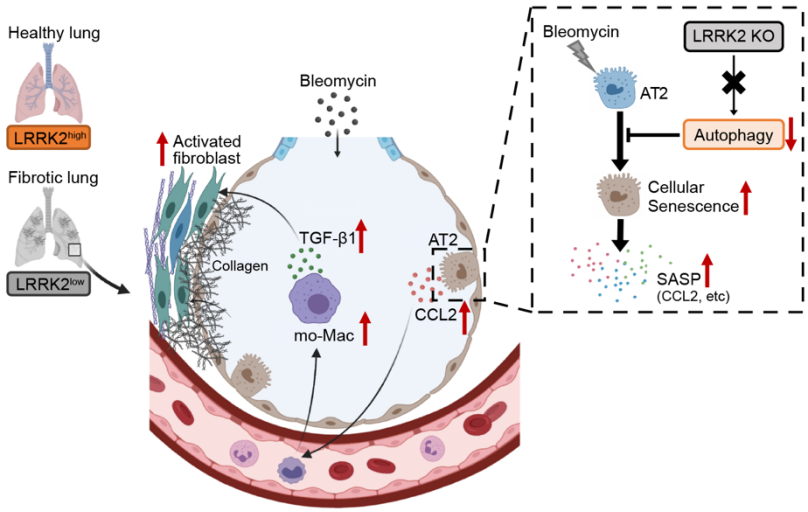

Fig. S13. Schematic diagram of the regulatory role of LRRK2 in the pathogenesis of pulmonary fibrosis. LRRK2, which was highly expressed in lung tissues of healthy human and mice, was significantly down-regulated in fibrotic lungs. In the classical mouse model of bleomycin-induced pulmonary fibrosis, LRRK2-deficient mice suffered from much more severe pulmonary fibrosis. Mechanistically, the loss of LRRK2 led to impaired autophagy and accelerated cellular senescence in AT2 cells. The senescent AT2 cells produced higher levels of chemokine CCL2, promoting the recruitment of mo-Macs and secretion of TGF-β1, which subsequently facilitated the activation and collagen secretion of lung fibroblasts. The illustration was created with BioRender.com.

Table S1. Antibody list for flow cytometry

Antibody	Clone	Source	Conjugates	Catalog No.
CD11b	M1/70	BioLegend	Brilliant Violet 605	101237
CD11b	M1/70	BioLegend	Brilliant Violet 711	101241
CD11c	N418	eBioscience	PE/Cy7	25-0114-82
CD11c	N418	eBioscience	FITC	11-0114-85
CD16/32	93	eBioscience	Purified	14-0161-82
CD19	eBio1D3	eBioscience	APC	17-0193-82
CD19	6D5	BioLegend	Pacific Blue	115523
CD24	M1/69	eBioscience	Purified	14-0242-82
CD24	M1/69	BioLegend	Brilliant Violet 605	101827
CD31	390	eBioscience	FITC	11-0311-82
CD31	390	eBioscience	PE/Cy7	25-0311-81
CD31	390	eBioscience	Purified	14-0311-82
CD3ε	eBio500A2	eBioscience	PE	12-0033-85
CD4	GK1.5	BioLegend	FITC	100406
CD45	30-F11	BioLegend	APC/Cy7	103116
CD45	30-F11	BioLegend	Purified	103102
CD8α	53-6.7	eBioscience	PE/Cy7	25-0081-82
EpCAM	G8.8	eBioscience	APC	17-5791-82
F4/80	BM8	eBioscience	APC	17-4801-82
F4/80	BM8	BioLegend	Brilliant Violet 421	123137
Ly6G	1A8	BD Biosciences	FITC	551460
Ly6G	1A8	BioLegend	Pacific Blue	127611
Ly6G	1A8	BioLegend	PE/Cy7	127617
MHC-II (I-A/I-E)	M5/114.15.2	BioLegend	FITC	107606
Podoplanin	8.1.1	eBioscience	PE	12-5381-80
Siglec-F	E50-2440	BD Biosciences	PE	552126
Siglec-F	E50-2440	BD Biosciences	Brilliant Violet 421	562681

Table S2. Primers used for qRT-PCR

Gene	Forward Primer (5'-3')	Reverse Primer (5'-3')
Lrrk2	GCTATCTTGCATTTCGTTGTGC	CCCAGGATTCCCAATGAACC
Acta2	GACGCTGAAGTATCCGATAGAACACG	CACCATCTCCAGAGTCCAGCACAAT
Fn1	TCTGGGAAATGGAAAAGGGGAATGG	CACTGAAGCAGGTTTCCTCGGTTGT
Col1a1	CCAAGAAGACATCCCTGAAGTCA	TGCACGTCATCGCACACA
Timp1	GCAAAGAGCTTTCTCAAAGACC	AGGGATAGATAAACAGGGAAACACT
Ctgf	GGGCCTCTTCTGCGATTTC	ATCCAGGCAAGTGCATTGGTA
Tnf	AGGCTGCCCCGACTACGT	GACTTTCTCCTGGTATGAGATAGCAAA
Il6	ACAAGTCGGAGGCTTAATTACACAT	TGCCATTGCACAACTCTTTT
Il1b	TCGCTCAGGGTCACAAGAAA	CATCAGAGGCAAGGAGGAAAAC
Chil3	TGTTCTGGTGAAGGAAATGCG	CGTCAATGATTCCTGCTCCTG
Arg1	CAGAAGAATGGAAGAGTCAG	CAGATATGCAGGGAGTCACC
Spp1	GGAGGAAACCAGCCAAGG	TGCCAGAATCAGTCACTTTCAC
S100a4	GGAGCTGCCTAGCTTCCTG	TCCTGGAAGTCAACTTCATTGTC
Retnla	CCTGCTGGGATGACTGCTACT	AGATCCACAGGCAAAGCCAC
Ccl2	TTAAAAACCTGGATCGGAACCAA	GCATTAGCTTCAGATTTACGGGT
Serpine1	CCTCTTCCACAAGTCTGATGGC	GCAGTTCCACAACGTCATACTCG
Mmp2	ATCGAGACCATGCGGAAGC	ATCCACGGTTTCAGGGTCC
Mmp10	GAGCCACTAGCCATCCTGG	CTGAGCAAGATCCATGCTTGG
Cd63	GAAGCAGGCCATTACCCATGA	TGACTTCACCTGGTCTCTAAACA
Ctsa	GCTGTCTCCACTGCTCTTGT	GTCCGATGCTCTGAGGTAGC
Ctsd	GCAGTGCCTCTTATCCAGGG	TGGGAGGGGGTATGTCCATT
Atp6v0e1	ATACCACGGCCTTACTGTGC	CAGAGGATTGAGCTGTGCCA
Atp6v1h	CACAGAAACTTCGTGGCAGC	CCAGGCAAACCGGTACTCAT
Actb	AGAGGGAAATCGTGCGTGAC	CAATAGTGATGATGACCTGGCCGT

SI References

1. R. H. Hübner, *et al.*, Standardized quantification of pulmonary fibrosis in histological samples. *Biotechniques* **44**, 507–517 (2008).
2. F. Saito, *et al.*, Role of interleukin-6 in bleomycin-induced lung inflammatory changes in mice. *Am. J. Respir. Cell Mol. Biol.* **38**, 566–571 (2008).
3. J. Lonsdale, *et al.*, The Genotype-Tissue Expression (GTEx) project. *Nat. Genet.* **45**, 580–585 (2013).
4. M. Uhlén, *et al.*, Tissue-based map of the human proteome. *Science (80-.).* **347** (2015).
5. A. I. Su, *et al.*, A gene atlas of the mouse and human protein-encoding transcriptomes. *Proc. Natl. Acad. Sci. U. S. A.* **101**, 6062–6067 (2004).
6. J. E. Lattin, *et al.*, Expression analysis of G Protein-Coupled Receptors in mouse macrophages. *Immunome Res.* **4**, 5 (2008).
7. C. Wu, *et al.*, BioGPS: An extensible and customizable portal for querying and organizing gene annotation resources. *Genome Biol.* **10**, R130 (2009).
8. F. A. Vieira Braga, *et al.*, A cellular census of human lungs identifies novel cell states in health and in asthma. *Nat. Med.* **25**, 1153–1163 (2019).
9. M. Cohen, *et al.*, Lung Single-Cell Signaling Interaction Map Reveals Basophil Role in Macrophage Imprinting. *Cell* **175**, 1031-1044.e18 (2018).